

NUMERICAL MODELLING OF COMPRESSION AFTER IMPACT RESPONSE OF WOVEN FIBER-REINFORCED COMPOSITES

Pedro Augusto Aparecido Eggert Mendes, pedroaaem@gmail.com

Mariano Andrés Arbelo, marbelo@ita.br

Maurício Vicente Donadon, donadon@ita.br

Sergio Frascino Muller de Almeida, frascino@ita.br

Instituto Tecnológico de Aeronáutica, DCTA – ITA, São José dos Campos, SP, Brazil. CEP: 12228-900.

Abstract. Recently a considerable effort has been dedicated towards the development of numerical and analytical models for CAI strength prediction in composite laminates. However, most of the models available in the open literature are very limited and they are unable to predict the complex interaction between different failure modes induced during the CAI tests. Within this context, this paper presents a numerical study on CAI residual strength prediction using energy based constitutive damage model. The damage model formulation combines continuum damage mechanics and fracture mechanics approaches within a unified way by using a smeared cracking formulation. The model was implemented into ABAQUS finite element code as an user defined material model within shell elements and validated against experimental results reported in the open literature. The damage model formulation allows the prediction of fiber failure and matrix cracking either in tension or compression, and an additional damage variable is also included into the formulation to account for in-plane shear failure at ply level. Delamination effects are also incorporated into the proposed modeling strategy by using a newly developed mixed-mode delamination contact-logic.

Keywords: Composites, CAI, Damage Model, Impact, Finite Elements

1. INTRODUCTION

High performance composite materials utilization and importance has grown over the years for the construction of primary structures in aerospace industry. The design of new aircrafts demands optimized and reliable lighter structures. Composite materials, such Carbon Fiber Reinforced Plastics (CFRP) have advantageous structural and manufacturing properties that can supply those necessities. However, CFRPs are inherently brittle and vulnerable to impact damage.

In low velocity impact the contact duration is sufficiently long enough for entire structure to respond and impact energy is absorbed elastically and/or eventually in damage creation. The resulting damage mechanism due to impact loading can be divided into four distinct categories: delamination, matrix cracking, fiber breakage and total perforation. For high velocity impact the damage is almost exclusively perforation and delamination of surrounding area (Donadon *et al.*, 2008). Based on that, ensure the structural integrity of aircraft components in the presence of low velocity impact damage is main concern of composite materials utilization. Compression After Impact (CAI) is the test methodology developed to evaluate the residual strength properties of multidirectional plates which have been previously subjected to indentation caused by an impact of weight drop, prior to the compressive loading.

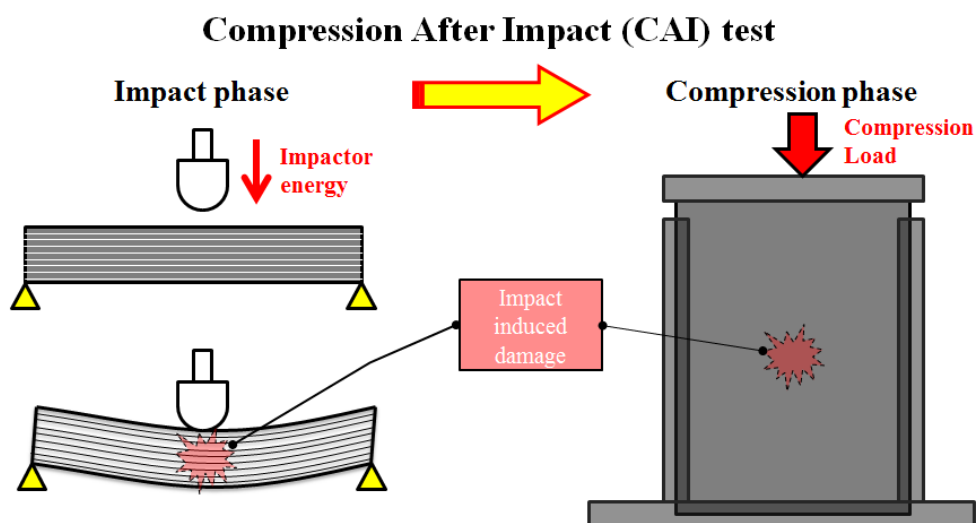


Figure 1. Schematically diagram of compression after impact test.

A considerable effort has been dedicated in the development of numerical and analytical models that can predict the CAI strength prediction and complex interactions between the failure modes that occurs. The finite element method becomes the most popular numerical method for impact modeling. The explicit formulation commercial codes, such as ABAQUS/explicit, have advanced contact procedure to deal with the wide range of contact problems, and a wide range of element formulation. Since the materials models plays a crucial rule for the damage formulation, the implementation of user defined subroutines to implement the constitutive models is another desirable characteristic for this application.

Yan, *et al.* (2010) investigated the CAI behavior of woven glass fiber-reinforced vinyl ester (glass/VE) panels using an eigendeformation-based reduced order computational homogenization (EHM) model to predicted the ply failure and compare the results against test results. The initial impact-induced damage was inferred from experimental observations using a conical representation of damaged area. The authors concluded that the delamination propagation of damaged coupons is critical to sublaminates buckling and leads to final shear failure. Soutis and Curtis (1996) studied several CFRP specimens and proposed a fracture toughness model to predict the CAI residual strength. The work showed the several types of impact-induced failures like delamination, fiber failure and splitting, and the evolution of delamination in the presence of compressive loads. The fracture toughness model predicts the CAI strength accurately for impacted coupons with certain failure characteristics.

Mendes *et al.* (2011) evaluated the CAI of CFRP coupons using a single shell finite element model with a proposed energy based damaged model implement as user defined material in ABAQUS explicit commercial package and for comparison purposes the Hashin failure model was also evaluated. The numerical results were compared against test results published in open literature. The proposed damage model showed better correlation for impact loads and compressive loads than the Hashin model. The CAI strength did not decrease for the higher impact energy coupons, since the shells elements formulation does not handle out-of-plane stress and strain that rules the delamination behavior.

Based on this scenario, this paper presents a new finite element model to predict the CAI of composite materials plated using an energy based constitutive damage model, that combines continuum damage mechanics and fracture mechanics approaches within a unified way by using a smeared cracking formulation. The damage model formulation allows the prediction of fiber failure and matrix cracking either in tension or compression, and an additional damage variable is also included into the formulation to account for in-plane shear failure at ply level. Delamination effects are also incorporated into the proposed modeling strategy by using a newly developed mixed-mode delamination contact-logic.

2. FINITE ELEMENT MODEL

In order to implement the delamination effects into the single shell model, as presented in Mendes *et al.* (2011), the laminate model was divided into two sublaminates shell models with half of original thickness and a 1/10 ply thick solid elements was inserted into the mid-plane defined between the two shell plates. Bonded contact formulation was used to connect the nodes of shell plates with the correspondent interface solid elements face nodes. Contact model between the shells plates was introduced to prevent penetration between components and distribute the out of plane compression loads correctly. During the impact phase, impactor has thought thickness contact capabilities. The model configuration is showed in Fig. 2 and the ABAQUS mesh details is depicted in Fig. 3.

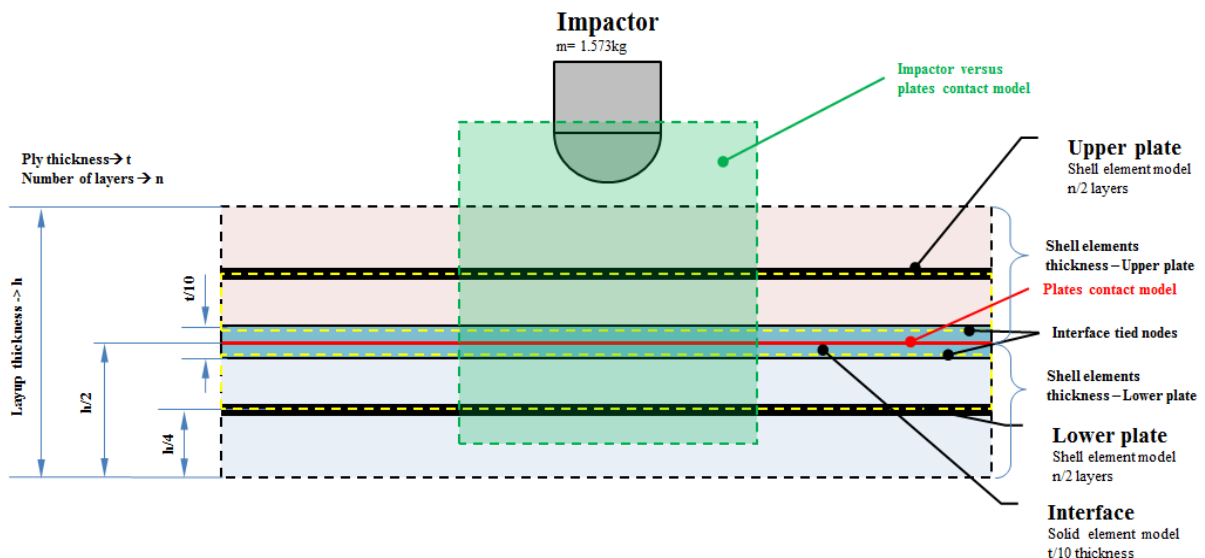


Figure 2. Proposed model details.

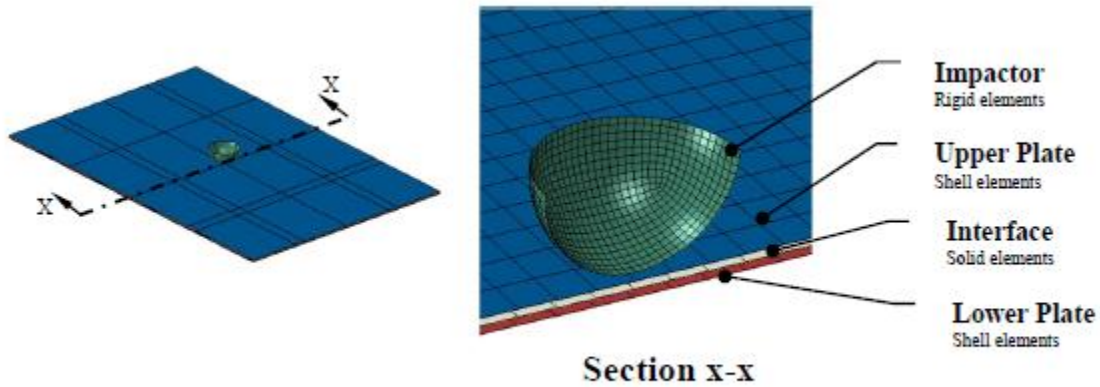


Figure 3. Proposed model mesh detail in ABAQUS.

3. CONTINUUM DAMAGE MECHANICS MODEL FOR COMPOSITE MATERIALS

The damage model proposed in this work was developed by Donadon and co-authors and several references are available in open literature (Donadon *et al.*, 2008, 2005, 2010; Yokoyama, *et al.*, 2010). The smeared cracking formulation is used to model progressive failure of composites. It relates the specific or volumetric energy, which is defined by the area underneath the stress-strain curve, with the strain energy release rate of the material. The method assumes a strain softening constitutive law for modeling the gradual stiffness reduction due to the micro-cracking process within the cohesive or process zone of the material. In order to avoid pathological problem associated with strain localization and mesh dependence during softening, the softening portion of a stress-strain curve is adjusted according to the element topology and cracking direction for each failure mode using an advanced objectivity algorithm (Donadon *et al.*, 2008).

3.1. Failure criteria

Equation (1) is the general form for all failure criteria used to detect damage initiation for all in-plane failure modes.

$$F_{ij}^k(\sigma_{ij}) = \frac{\sigma_{ij}}{S_{ij}^k} - 1 \geq 0 \quad (1)$$

where k refers to the associated failure modes ($k = t$ for failure in tension, $k = c$ for failure in compression and $k = s$ for failure in shear). The subscripts ij indicate the failure direction ($i = j = 1$ for fiber direction, $i = j = 2$ for matrix direction and $i \neq j$ for shear direction). S_{ij}^k is the maximum stress in ij direction for k failure mode and σ_{ij} is the acting stress on each layer of the material's local coordinate system.

3.2. Damage evolution laws

Once the failure criteria are met, the damage commences and grows according the damage evolution laws defined below.

3.2.1 Damage evolution law for fiber failure and matrix cracking

Equation (2) is the general expression for damage evolution laws in the fiber and matrix.

$$d_{ii}(\lambda_{i,1}, \lambda_{i,2}) = \lambda_{i,1} + \lambda_{i,2} - \lambda_{i,1}\lambda_{i,2} \quad (2)$$

with

$$\lambda_{i,1} = \frac{2G_{ii}^t}{2G_{ii}^t - S_{ii}^t \varepsilon_{i,0}^t} \left(\frac{\varepsilon_{ii}^t - \varepsilon_{i,0}^t}{\varepsilon_{ii}^t} \right) \quad (3)$$

$$\lambda_{i,2} = \frac{2G_{ii}^c}{2G_{ii}^c - S_{ii}^c l^* \varepsilon_{i,0}^c} \left(\frac{\varepsilon_{ii}^c - \varepsilon_{i,0}^c}{\varepsilon_{ii}^c} \right) \quad (4)$$

where $i=1$ for fiber cracking and $i=2$ for matrix cracking. The values for both functions $\lambda_{i,1}, \lambda_{i,2} \in [0,1]$. G_{ii}^t and G_{ii}^c are the intralaminar fracture toughnesses in tension and compression, respectively. $\varepsilon_{i,0}^t$ and $\varepsilon_{i,0}^c$ are maximum strains prior to catastrophic failure in tension and compression, respectively. In order to account for damage irreversibility effects $\varepsilon_{ii}^k = \max \left[\left| \varepsilon_{ii}^{\max}(t) \right|, \varepsilon_{i,0}^k \right]$ where $\varepsilon_{ii}^{\max}(t)$ is the maximum achieved strain in the strain versus time history. The superscript k refers to the fiber failure mode, that is, $k=t$ for failure in tension and $k=c$ for failure in compression. The characteristic length l^* is used for mapping the material process (or microcracking) zone into the finite element mesh. For fiber failure modes l^* is computed in terms of the isoparametric coordinates (ξ_m, η_m) for each integration point m according to the following expression,

$$l^*(\xi_m, \eta_m) = \left(\sum_{i=1}^{n_c} \left[\frac{\partial N_i(\xi_m, \eta_m)}{\partial x} \cos(\theta_m) + \frac{\partial N_i(\xi_m, \eta_m)}{\partial y} \sin(\theta_m) \right] \phi_l \right)^{-1} \quad (5)$$

where $\theta_m = \theta_{\text{fibre}}$ being θ_{fibre} the fiber orientation angle for each integration point for fiber failure and $\theta_m = \theta_{\text{fibre}} + 90^\circ$ for failure in the matrix direction. For four nodes shell elements $n_c = 4$, $N_i(\xi_m, \eta_m)$ are bi-linear interpolation functions and ϕ_l is defined as crack band discontinuity function. Details about the derivation of the expression for the characteristic length for orthotropic smeared cracking modes can be found in Donadon *et al.* (2008).

3.2.2 Damage evolution law for in-plane shear failure

The damage evolution for in-plane shear failure is given by

$$d_{12}(\gamma_{12}) = \frac{\gamma_{12,f} \left[2(\gamma_{12} - \gamma_{12,0}^m) - \gamma_{12,f} \right]}{(\gamma_{12,f} + \gamma_{12,0}^m - \gamma_{12})(\gamma_{12} - \gamma_{12,0}^m)} \quad (6)$$

with

$$\gamma_{12,f} = \frac{2G_s}{S_{12} l^*} \quad (7)$$

where $\gamma_{12,0}^m$ is the inelastic strain at failure and G_s is the in-plane shear intralaminar fracture toughness. The characteristic length l^* for in-plane shear failure is assumed to be the same as the one used for fiber failure modes (Donadon *et al.*, 2010).

3.3 Non-linear rate dependent in-plane shear model

The in-plane shear behavior is modeled using a rate depended constitutive model and accounts for shear nonlinearities, irreversible strains and damage within the Representative Volume Element (RVE) of the material (Donadon and Iannucci, 2006). It is defined as follows,

$$\tau_{12} = \alpha G_{12} \gamma_{12} \quad (8)$$

with

$$G_{12} = G_{12}^0 + c_1 \left(e^{-c_2 \gamma_{12}} - 1 \right) \quad (9)$$

where G_{12}^0 is the initial shear modulus and c_1 and c_2 are material constants obtained from in-plane shear tests. α is the strain-rate enhancement given by the following law,

$$\alpha = 1 + e^{\frac{\dot{\gamma}_{12}}{c_3}} \quad (10)$$

where c_3 is a material constant obtained from dynamic in-plane shear tests. Equation 11 defines the inelastic shear strain γ_{12}^{in} in terms of the elastic shear strain γ_{12}^e and total shear strain γ_{12} .

$$\gamma_{12}^{in} = \gamma_{12} - \gamma_{12}^e = \gamma_{12} - \frac{\tau_{12}(\gamma_{12})}{G_{12}^0} \quad (11)$$

3.4 Stress degradation procedure

The resultant degraded stresses at ply level are given by

$$\begin{Bmatrix} \sigma_{11}^d \\ \sigma_{22}^d \\ \tau_{12}^d \end{Bmatrix} = \begin{bmatrix} [1 - d_{11}(\lambda_1^f, \lambda_2^f)] & 0 & 0 \\ 0 & [1 - d_{11}(\lambda_1^f, \lambda_2^f)][1 - d_{22}(\lambda_1^m, \lambda_2^m)] & 0 \\ 0 & 0 & [1 - d_{12}(\gamma_{12})] \end{bmatrix} \begin{Bmatrix} \sigma_{11} \\ \sigma_{22} \\ \tau_{12} \end{Bmatrix} \quad (12)$$

where

$$\begin{Bmatrix} \sigma_{11} \\ \sigma_{22} \\ \tau_{12} \end{Bmatrix} = \frac{1}{(1 - \nu_{12}\nu_{21})} \begin{bmatrix} E_{11} & \nu_{12}E_{22} & 0 \\ \nu_{21}E_{11} & E_{22} & 0 \\ 0 & 0 & G_{12} \end{bmatrix} \begin{Bmatrix} \varepsilon_{11} \\ \varepsilon_{22} \\ \gamma_{12} \end{Bmatrix} \quad (13)$$

4. INTERFACE/SUBLAMINATE DEBONDING CONTACT LOGIC

The contact-logic is defined in terms of tractions and relative displacements between the upper and lower surfaces defining the interface. The relative displacement vector is composed of the resultant normal and sliding components defining by the relative movement between upper and lower surfaces of the contact element (see Fig. 4 (a)). The criteria for damage initiation and damage progression are respectively given by Eq. (14) and (15). The constitutive law for a three dimensional stress case is shown in Fig. 4 (c). G_i is the strain energy released rate defined by Eq. (16). K_{ii} is the interfacial stiffness in the direction ii , for $i = I, II, III$, and d is the damage parameter defined in Eq. (25). The mixed-mode delamination damage onset displacement vector is given in Eq. (17), and the final resultant displacement associated with the fully debonded interfacial behavior, is given in Eq. (18), α and β are defined in Fig. 4 (b), and they are the angles that define the orientation of the resultant relative displacement vector. Details about the formulation are given in Donadon, *et al.* (2009).

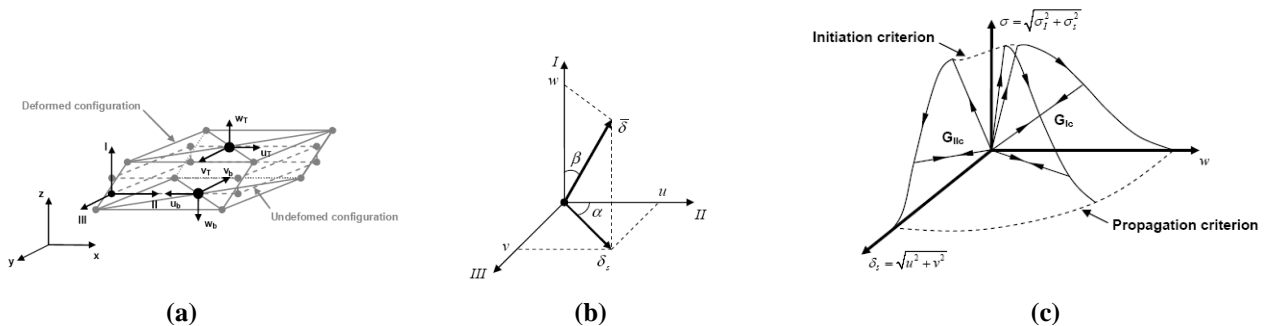


Figure 4. Contact-logic: (a) 3D contact element, (b) Resultant displacement vector, (c) Constitutive law

$$\left(\frac{\sigma_I}{N}\right)^2 + \left(\frac{\sigma_{II}}{S_{II}}\right)^2 + \left(\frac{\sigma_I}{S_{III}}\right)^2 = 1 \quad (14)$$

$$\left(\frac{G_I}{G_{Ic}}\right)^{\lambda} + \left(\frac{G_{II}}{G_{IIc}}\right)^{\lambda} + \left(\frac{G_I}{G_{IIIc}}\right)^{\lambda} = 1 \quad (15)$$

$$G_i = \int_0^{\delta_f} \sigma_i d\delta_i \rightarrow \sigma_i = K_{ii}(1-d)\delta_i \quad (16)$$

$$d = 1 - \frac{\bar{\delta}_0}{\bar{\delta}} \left[1 + \left(\frac{\bar{\delta} - \bar{\delta}_0}{\bar{\delta}_f - \bar{\delta}_0} \right)^2 \left(2 \left(\frac{\bar{\delta} - \bar{\delta}_0}{\bar{\delta}_f - \bar{\delta}_0} \right) - 3 \right) \right] \text{ with } \bar{\delta} = \sqrt{u^2 + v^2 + w^2} \quad (17)$$

$$\bar{\delta}_0 = \left[\left(\frac{K_{ww} \cos(\beta)}{N} \right)^2 + \left(\frac{K_{uu} \sin(\beta) \cos(\alpha)}{S_{II}} \right)^2 + \left(\frac{K_{vv} \sin(\beta) \sin(\alpha)}{S_{III}} \right)^2 \right]^{-1/2} \quad (18)$$

$$\bar{\delta}_f = \frac{2}{\bar{\delta}_0} \left[\left(\frac{K_{ww} \cos(\beta)}{G_{Ic}} \right)^2 + \left(\frac{K_{uu} \sin(\beta) \cos(\alpha)}{G_{Ic}} \right)^2 + \left(\frac{K_{vv} \sin(\beta) \sin(\alpha)}{G_{IIIc}} \right)^2 \right]^{-1/2} \quad (19)$$

5. IMPACT AND CAI SIMULATION RESULTS

5.1 Model Parameters

Table 1 presents the material properties for the 150x100x2mm³ CFRP plate coupons used for the impact and compression after impact simulations. The boundary conditions used for the two sequential steps are presented in Fig. 4.

Table 1. Material properties for 2mm plate thickness.

Lay-up [$\pm 45^\circ/(0^\circ, 90^\circ)/\pm 45^\circ/(0^\circ, 90^\circ)/\pm 45^\circ$] _s					
Elastic Properties [GPa]		Ply strengths [MPa]		Intralaminar fracture toughness [kJ/m ²]	
E ₁₁	60.80	X _t	621	G _{ft}	75
E ₂₂	58.25	X _c	760	G _{fc}	25
G ₁₂	4.55	Y _t	594	G _{mt}	2.5
Poisson ratio [-]		Y _c	707	G _{mc}	2.5
v ₁₂	0.07	S ₁₂	125	G _{st}	2.25

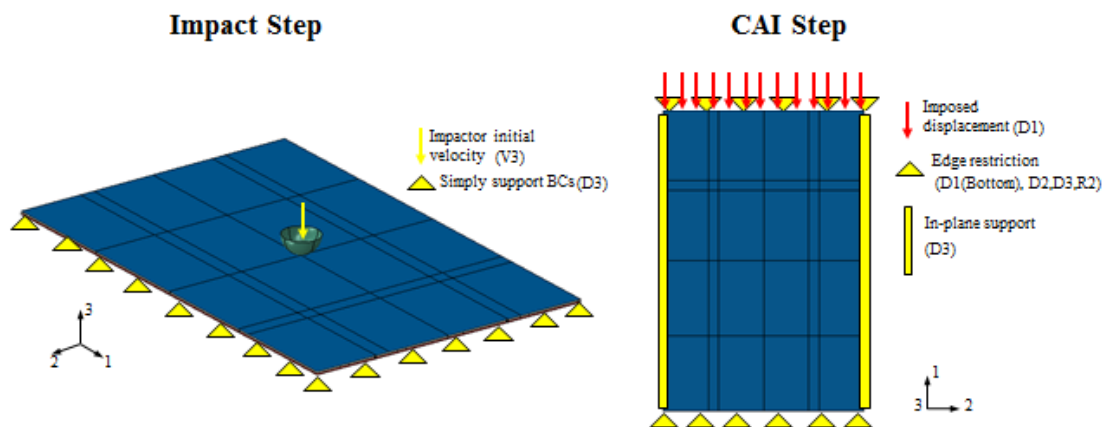


Figure 4. Simulation steps boundary conditions (“D” for displacement BCs, “V” for velocity BCs, “R” for rotations BCs).

5.2 Impact Results

Biase (2009) in his work, showed good correlation comparing impact test results against finite element simulations using only single shell model. In order to verify the accuracy of the proposed model, the impact energy loadcases were simulated and the results were compared with previous results. The results can be seen in Table 2.

Table 2. Impact load results comparison.

Impact energy	Model	Impact duration [ms]	Impact peak load [kN]	Peak load time [ms]	Experimental peak load results difference [%]
8J	IM	6.497	2.605	2.561	4%
	SSM	6.680	2.699	-	8%
	Test	6.400	2.500	-	-
16J	IM	6.905	3.095	2.794	4%
	SSM	6.420	4.048	-	36%
	Test	7.280	2.973	-	-
28J	IM	-	3.126	1.614	4%
	SSM	5.920	5.595	-	86%
	Test	3.180	3.009	-	-

IM= Interface model
 SSM = Single shell model

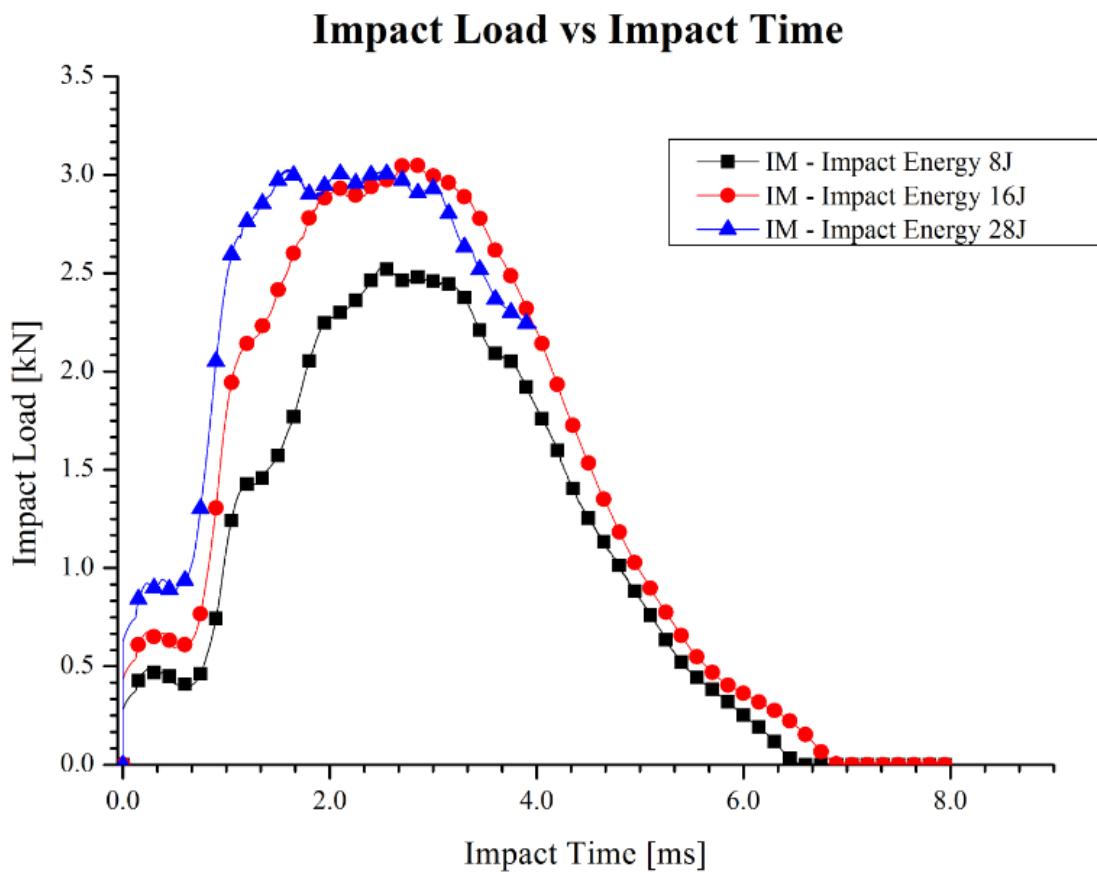


Figure 5. Impact load versus impact time curves.

Comparisons between the numerical and experimental damage patterns for different impact scenarios are shown in Fig. 6. The delaminated area for each impact energy can be seen in Fig. 7.

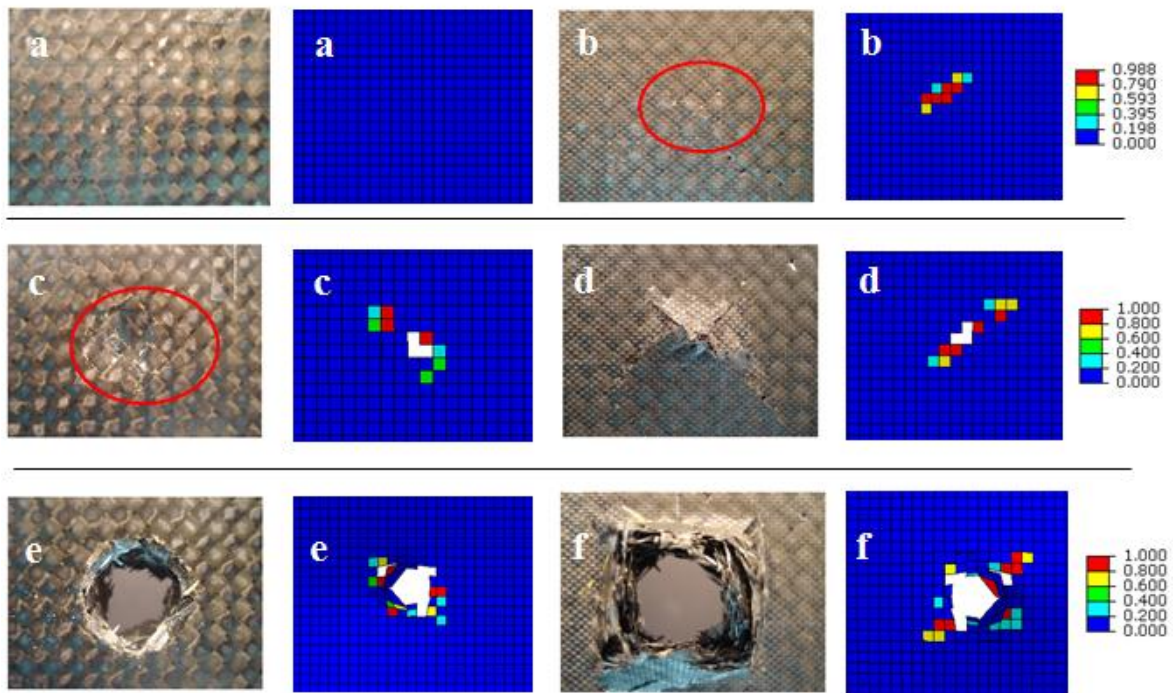


Figure 6. Comparative visual damage between test specimens and finite element model. Fiber failure fringe plot. (a,b) upper and bottom face for 8J impact, respectively; (c,d) upper and bottom face for 16J impact, respectively; (e,f) upper and bottom face for 28J impact, respectively.

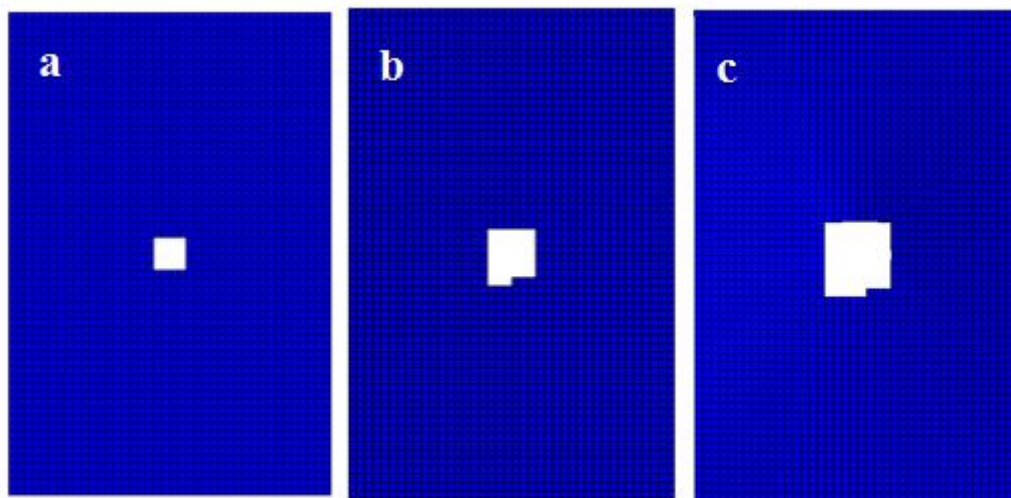


Figure 7. Delaminated area for (a) 8J impact; (b) 16J impact; (c) 28J impact.

5.3 Compression Results

CAI simulations were carried out for laminates subjected to two distinct impact energy levels, 8 and 16 Joules. A non-impacted plate was also considered for comparison purposes. Figure 8 shows the compression load versus displacement results. In terms of CAI tests, the results were no satisfactory, since the model and the tested specimens buckled with a load near half of the ultimate compression load. However the model predicted with some accuracy the buckling loads and the ultimate loads for these tests. The ultimate load reduction caused by the impact damage was not so evident, but it can be noticed (Tab. 3). The experimentally observed failure modes for the non-impacted coupons were very similar to the ones predicted by the finite element model (Fig. 9)

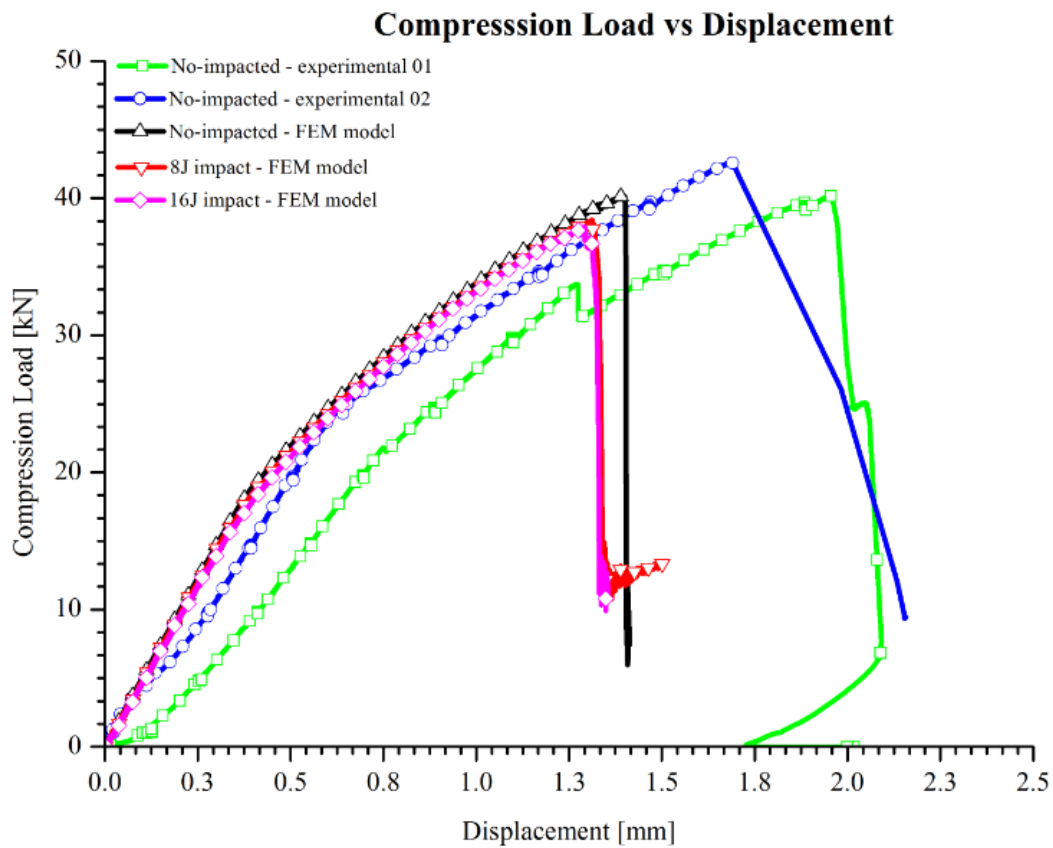


Figure 8. Compression loads for simulation and test.

Table 3. Ultimate compression load comparison.

		Experimental Results			
FEM Results	Ultimate Load[kN]	No-impacted - experimental 01	No-impacted - experimental 02	Experimental Average	
			40.17	42.68	41.43
No-impacted - FEM model	40.22	0%	6%	3%	FEM/ Experimental Difference
8J impact - FEM model	38.41	5%	% Compression load capacity reduction		
16J impact - FEM model	37.91	6%			

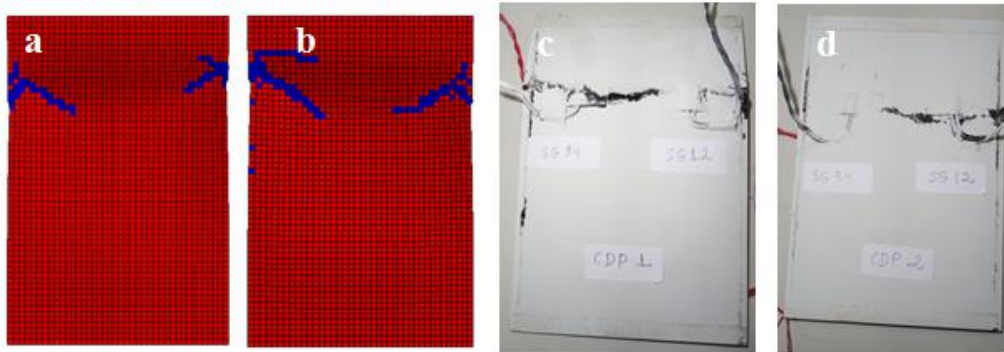


Figure 9. Failure plot comparison against no-impacted coupons.(a,b) are the front and back face of plate; (c) is the No-impacted - experimental 01 specimen and (d) No-impacted - experimental 02 specimen.

6. CONCLUSION

The new proposed model containing the contact-logic and sub-laminates provided better results compared to previous published results, for impact simulation and for compression after impact. The tested coupons are very thin to be tested in the conventional CAI device. An anti-buckling device will be designed and implemented for future validation. New FEM models will be studied to improve the tests and simulation correlations.

7. REFERENCES

- Biase, E. C. B., 2009, “Análise estrutural de laminados compósitos sujeitos a cargas de impacto”, MsC Thesis, Instituto Tecnológico de Aeronáutica, São José dos Campos, Brasil, 190p.
- Donadon, M.V., 2005 “The impact behavior of composite structures manufactured using resin infusion under flexible tooling”, Ph.D Thesis, Department of Aeronautics, Imperial College London, England, UK, 375 p.
- Donadon, M. V. and Iannucci L., 2006 “Bird strike modeling using a new woven glass failure model”, Proceedings of the LS-DYNA International Conference, Michigan, Dearborn, USA.
- Donadon, M.V., Iannucci,L., Falzon, B.G., Hodgkinson, J.M., de Almeida, S.F.M., 2008, “A progressive failure model for composite laminates subjected to low velocity damage”, *Computers & Structures*, 86, pp.1232-1252.
- Donadon M.V., de Almeida S.F.M., Arbelo M. A., 2009, “A contact logic for mixed mode delamination modelling in composite laminates”, to be published in an International Journal.
- Donadon, M.V., Arbelo, M.A., de Almeida, S.F.M., Actis, M., Pantanella, A.J., 2010, “Bird strike modeling in composites stiffened panels”, Proceedings of 11th Pan-American Congress of Applied Mechanics”, Foz do Iguaçu, Brazil.
- Freitas, M., Reis, L., 1998, “Failure mechanisms on composite specimens subjected A progressive failure model for composite laminates subjected to compression after impact”, *Computers & Structures*, 42, pp.365-373.
- Mendes, P.A.A.E., Donadon, M.V., de Almeida, S.F.M., 2011, “Numerical prediction of CAI strength of composite laminates”, Proceedings of 5th International Conference on Composites Testing and Model Simulation”, Lausanne, Switzerland, pp.17-18.
- Soutis, C., Curtis, P.T., 1996, “Prediction of the post-impact compressive strength of CFRP laminate composite”, *Composites Science and Technology*, 56, pp.677-687.
- Yan, H., Oskay, C., Krishnan, A., Xu, L.R., 2010, “Compression-after-impact response of woven fiber-reinforced composites”, *Composites Science and Technology*, 70, pp.2128-2136.
- Yokoyama, N. O., Donadon, M.V., de Almeida, S.F.M., 2010, “A numerical study on the impact resistance of composite shells using an energy based failure model”, *Computers & Structures*, 93, pp.142-152.

8. RESPONSIBILITY NOTICE

The following text, properly adapted to the number of authors, must be included in the last section of the paper:
The author(s) is (are) the only responsible for the printed material included in this paper.